

## Article

# Analysis of Spatiotemporal Transmission Characteristics of African Swine Fever (ASF) in Mainland China

Xin Pei <sup>1,\*</sup>, Mingtao Li <sup>1</sup>, Jianghong Hu <sup>2</sup>, Juan Zhang <sup>2</sup> and Zhen Jin <sup>2,\*</sup><sup>1</sup> School of Mathematics, Taiyuan University of Technology, Taiyuan 030024, China<sup>2</sup> Complex System Research Center, Shanxi University, Taiyuan 030006, China

\* Correspondence: peixin1120@126.com (X.P.); jinzhn@263.net (Z.J.)

**Abstract:** In view of the rapid spread of African swine fever in Mainland China from 2018 to 2019, we used spatiotemporal statistical analysis methods to study the spatiotemporal transmission features of African swine fever. The results reveal that the hot spots of African swine fever were concentrated in some cities in Northeast and Southwest China. Seven spatiotemporal clusters of African swine fever were identified, and the most likely spatiotemporal cluster was located in the Buyi and Miao Autonomous Prefecture of QianNan in Guizhou Province, and the cluster date was from 19 June to 25 June 2019. The first secondary cluster covered five cities (Shenyang, Yingkou, Panjin, Anshan, and Liaoyang) in Liaoning Province from 1 August to 10 October 2018. In addition, from the global and local transmission direction and speed of African swine fever in Mainland China, the spatial transmission speed of ASF was found to be slow from August to October 2018, and fast from February to March 2019. Lastly, the global and local isolation and exposure of sites infected with ASF were calculated in Mainland China to reveal the infection risk of different susceptible sites and time periods.

**Keywords:** African swine fever; hot spots; spatiotemporal cluster; diffusion direction and speed; isolation and exposure

MSC: 37M05



**Citation:** Pei, X.; Li, M.; Hu, J.; Zhang, J.; Jin, Z. Analysis of Spatiotemporal Transmission Characteristics of African Swine Fever (ASF) in Mainland China. *Mathematics* **2022**, *10*, 4709. <https://doi.org/10.3390/math10244709>

Academic Editor: Yuri V. Tyutyunov

Received: 21 October 2022  
Accepted: 9 December 2022  
Published: 12 December 2022

**Publisher's Note:** MDPI stays neutral with regard to jurisdictional claims in published maps and institutional affiliations.



**Copyright:** © 2022 by the authors. Licensee MDPI, Basel, Switzerland. This article is an open access article distributed under the terms and conditions of the Creative Commons Attribution (CC BY) license (<https://creativecommons.org/licenses/by/4.0/>).

## 1. Introduction

African swine fever (ASF) is a highly infectious and fatal disease caused by the African swine fever virus (ASFV) and currently has no specific treatment or vaccine [1]. The disease was first introduced to China in August 2018, and by 31 August 2019, it spread throughout Mainland China [2]. The rapid spread of African swine fever in China resulted in the culling of more than a million pigs, which has caused a huge impact on the pig market and pig products, thus causing great economic losses. Therefore, clarifying the transmission characteristics of African swine fever in Mainland China for different locations and time periods, and preventing and controlling the disease scientifically and efficiently are particularly important.

Statisticians have proposed many statistical methods to analyze the spatial and temporal distribution characteristics of the disease. As early as 1950, Moran put forward the global Moran's I index to quantitatively describe the global autocorrelation between the same data at different locations. In 1973, Cliff and Ord proposed a detailed procedure for statistical testing using Geary's C to evaluate the spatial dependence of data [3]. Moran's I and Geary's C can both determine the spatial distribution pattern of attributes (discrete, clustered or random). In 1992, Getis and Ord proposed the statistical index Getis-Ord  $G_i^*$  to calculate the spatial clustering locations of high-value or low-value elements, namely the distribution of hot spots and cold spots [4]. Based on the global Moran's I index, Anselin proposed the local Moran's I index to distinguish the spatial cluster and outlier of elements with high or low values [5].

In recent years, some statistical methods have been applied to analyze the spatiotemporal features of African swine fever spread, and have achieved some significant results.

For example, Zakharova et al. analyzed the genotype of ASF virus and the spatiotemporal characteristics of ASF cases in the Russian Far East from 2019 to 2020, applying spatiotemporal analysis with the space–time permutations model [6]. Blokhin et al. identified the potential clusters and hot spots of ASF in wild boar and domestic pigs in the Russian Federation from 2017 to 2019, based on the spatiotemporal scanning statistics of the Kulldorff and Mann-Kendall statistics methods [7]. Shao et al. used a spatial direction analysis and spatiotemporal scan statistics to research the spatial diffusion direction and spatiotemporal cluster features of African swine fever in Vietnam from February 2019 to March 2022 [8]. Andraud et al. investigated the spatiotemporal features and risk agricultural factors of ASF outbreaks in Romania from 2018 to 2019, applying a spatiotemporal clustering and random forest methodology. Their research results underscore the importance of strict biosafety measures on pig farms and during transportation [9]. African swine fever first occurred in China in August 2018; since then, experts have carried out relevant research on its space–time propagation characteristics. Ma et al. applied the spatiotemporal cluster and directional distribution analysis methods to study the distribution characteristics and high-risk areas of ASF cases in China from 1 August 2018 to 1 January 2019, and presented a disease risk map to provide recommendations for the effective prevention and control of ASF outbreaks [10]. Zhang et al. revealed which locations in China are prone to ASF occurrence based on a multi-criteria decision analysis (MCDA) and the weighted linear combination (WLC) method. The results provided support to Chinese veterinary departments in implementing monitoring and control measures for ASF [11]. However, more time–space transmission characteristics are worth analyzing to provide effective suggestions for the prevention and control of ASF in China, such as hot spots, propagation direction, propagation speed, etc.

In this paper, we collect surveillance data on African swine fever from 1 August 2018 to 31 August 2019 and perform data crawling on the location data of pig farms and slaughterhouse locations from Baidu Map. Based on these data, we study the spatial distribution pattern of African classical swine fever and determine the hot spots where this disease occurs using spatial autocorrelation analysis. Then, we determine the aggregation time and corresponding aggregation region of the disease through the spatiotemporal scanning statistical method. In addition, a trend surface analysis is used to study the overall and local transmission direction and speed of disease. Kriging interpolation is used to infer high-risk and potential high-risk areas of diseases at different times. Finally, we analyze the infection risk of susceptible sites for different locations and time periods by calculating isolation and exposure indicators. These research results can provide targeted references for the prevention and control of African swine fever in China in different locations and time periods.

## 2. Materials and Methods

### 2.1. Study Area and Data Sources

**Study area:** In this study on the direction and speed of diffusion and on the global spatial isolation and exposure of ASF, we take Mainland China as the spatial study area, including its 23 provinces, 4 municipalities, and 5 autonomous regions. For the analysis of other spatiotemporal features, the spatial study area focuses on Liaoning Province, in addition to all of Mainland China, as the first case and the largest number of ASF pig farm cases occurred in Liaoning Province. Liaoning Province is one of the northeast inland provinces of China situated between 118° and 125° east longitude and between 38° and 43° north latitude. Liaoning Province has 14 prefecture-level cities, 16 county-level cities, 25 counties, and 59 municipal districts. In addition, the time period analyzed in this study is from 1 August 2018 to 31 August 2019. The study units used in the cluster and outlier, hot spot, and spatiotemporal clustering analyses were administrative-level cities, while those in all other studies conducted here were county- or district-level cities.

**Data for African swine fever cases:** We collected the surveillance data on ASF in Mainland China from the Ministry of Agriculture and Rural Affairs of the People's Republic of China (<http://www.moa.gov.cn/>, accessed on 31 August 2019) with the study period

covering from 1 August 2018 to 31 August 2019. They include the the date of disease onset, the date of the report, the number of live pigs in stock, the geographical location, disease and death at the time of disease reporting. The research objects in this paper are all pig farm or slaughterhouse, and the African swine fever cases mentioned all had their disease onset at these pig farms and slaughterhouses, and no special explanation will be given afterwards.

Data for the pig farm and slaughterhouse: The total number of pig farms or slaughterhouses for each city was based on the statistics published in the China Animal Husbandry and Veterinary Yearbooks (2018) and Statistical Yearbook (2018) for each province. Moreover, we collected the information on each pig farm and slaughterhouse from Baidu Map using Python language. The Python language search terms included “geographical name”, “pig farm, pig farmer, pig farming cooperative”, and “slaughterhouse, slaughterhouse”. The extracted results include data on the names and the longitude and latitude for all sites.

### 2.2. Spatial Analytical Framework

The framework of the specific research method is shown in Figure 1. First, the global space autocorrelation method was used to describe the entire spatial distribution mode of the ASF case. The local means of spatial autocorrelation with cluster and outlier analysis (Anselin Local Moran’s  $I$ ) and hot spot analysis (Getis–Ord  $G_i^*$ ) were applied to obtain the spatial distribution characteristics. Then, we used the spatiotemporal statistical analysis method to analyze the spatiotemporal clusters areas of ASF. Furthermore, the trend surface analysis method was used to compute the global and local transmission direction and speed. In addition, we used Kriging interpolation to infer the high-risk and potentially high-risk regions of ASF at different times. Lastly, the risk of infection for different locations and time periods at the susceptible sites was studied by calculating the isolation and exposure index.

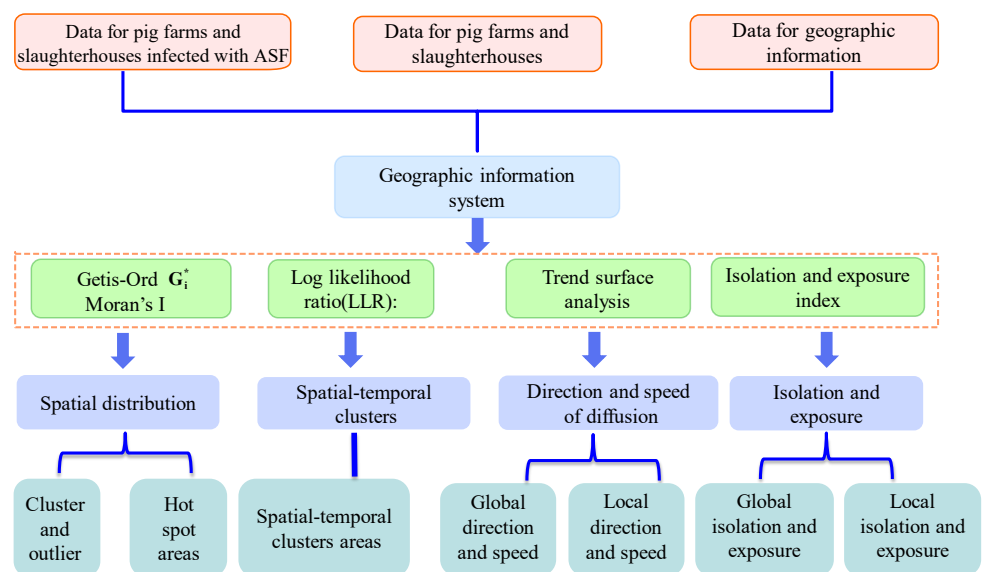


Figure 1. Technical analysis flowchart.

**Global spatial autocorrelation.** Spatial autocorrelation analysis is a spatial statistical method that reveals the regional structure of spatial variables, including global and local spatial autocorrelation [12,13]. In a global spatial autocorrelation analysis, the most commonly used statistical index is global Moran’s  $I$  index, which is mainly used to describe the average degree of association between all spatial units and the surrounding areas in the whole region [14]. Moran’s  $I$  index is usually used to describe global spatial autocorrelation. The range of Moran’s  $I$  value is  $[-1, 1]$ , where Moran’s  $I > 0$  indicates a positive autocorrelation, Moran’s  $I < 0$  indicates negative autocorrelation, and Moran’s  $I = 0$  indicates no correlation. In this study, the global Moran’s  $I$  index was used to investigate the spatial correlation of African swine fever cases at the urban level in China and to analyze

the clustering trend of the spatial distribution of African swine fever cases in China. The formula for global Moran’s  $I$  is presented in Appendix A.1.

**Cluster and outlier analysis.** Local Moran’s  $I$  can be further used to clarify the model and exact position of the cluster between local clusters [5]. At the level of statistical significance, Moran’s  $I_i > 0$  indicates that adjacent spatial locations surrounding the area  $i$  have similar attribute values, that is, either the cluster has high values or the cluster has low values; Moran’s  $I_i < 0$  implies that adjacent spatial locations surrounding the area  $i$  have non-similar attribute values, that is, spatial outliers. The statistical significance of the four spatial-related modes are expressed: high–high clusters (HH), low–low clusters (LL), high–low clusters (HL), and low–high clusters (LH). High clusters (that is, high-infection areas surrounded by other high-infection areas) are the most important model for preventing diseases and control purposes [15]. The formula for local Moran’s  $I$  is presented in Appendix A.2.

**Hot spot analysis.** Getis–Ord  $G_i^*$  can be used to identify the distribution of hot spots and cold spots, that is, to determine high-infection areas and low-infection areas [16]. The Getis–Ord  $G_i^*$  statistic itself is a statistical test of the  $Z$ -score. At the level of statistical significance,  $Z > 0$  refers to a high-value clustering category, where higher scores mean higher clustering;  $Z < 0$  refers to a cold point area, where lower negative  $Z$ -scores indicate that the low-value clustering class is stronger; and a  $Z$ -score close to 0 indicates a lack of a spatial cluster, suggesting that the disease is randomly distributed. The Getis–Ord formula for  $G_i^*$  is introduced in Appendix A.3.

**Spatiotemporal clustering analysis.** We use Kulldorff’s space–time scan statistic analysis method to detect the spatiotemporal clusters of ASF cases at the city, district, or county levels based on the discrete Poisson probability model [17]. The idea behind this method is the use of dynamic cylindrical Windows to scan different time periods and geographical regions to detect all possible clusters. The specific technical operation involves creating a two-dimensional scanning cylinder on the map. The center at the bottom of the cylinder moves between the center points of each region, and the radius at the bottom represents the included total population at risk, varying between 0 and the set maximum total population at risk. The height of the cylinder represents the interval between scans. The bottom center, bottom radius, and height of the cylinder window constantly change. For each location and size of the scanning window, we calculate the relative risk ( $RR$ ) using the ratio of the observed number of cases to the expected number of cases inside and outside the window and calculate the log likelihood ratio ( $LLR$ ) using the likelihood function [18]. In the space–time scan analysis in this paper, the spatial component is a city or county, and the temporal component is day of the week. The spatial size of the scan window was limited to a percentage of the total population at risk, where the total population is the total number of pig farm and slaughterhouse. The temporal size was set to a specific percentage of the total study period in order to scan clusters from small to large.

The formula for  $RR$  at a given window is as follows:

$$RR = \frac{n/E(n)}{(N - n)/(N - E(n))}. \tag{1}$$

The formula for  $LLR$  at a given window is as follows:

$$LLR = \log\left(\frac{n}{E(n)}\right)^n \left(\frac{N - n}{N - E(n)}\right)^{N - n} I^*. \tag{2}$$

where  $N$  is the total number of infected pig farm and slaughterhouse;  $n$  is the observed number of infected pig farm and slaughterhouse within the scan window;  $E(n)$  and  $N - E(n)$  are the expected number of infected pig farm and slaughterhouse within and outside the scan window under the null hypothesis (the spatiotemporal clustering of the study area are caused by random factors), respectively; and  $I^*$  is the indicator function, with  $I^* = 1$  when the window has more cases than expected under the null hypothesis and  $I^* = 0$  otherwise.

The statistical significance, the  $p$  value, for identified clusters was evaluated based on Monte Carlo hypothesis testing using the Poisson probability model option in SaTScan with 999 simulations. For all location and sizes of the scanning window, we can calculate the value of log likelihood ratio ( $LLR$ ). At the level of statistical significance, the window with the maximum  $LLR$  is assumed to be the most likely cluster, while the other windows with a statistically significant  $LLR$  are defined as secondary clusters ranked by their  $LLR$  value. The magnitude of  $LLR$  value reflects the intensity of clustering, and the greater the  $LLR$  value, the greater the possibility of clustering of cases in the clustering area. The spatiotemporal clustering analysis was conducted in the SaTScan version 9.6 software (<https://www.satscan.org/>, accessed on 31 August 2019), and the results were visualized in ArcGis 10.2.

**Trend surface analysis.** We used the trend surface analysis (TSA) method to explore the direction and speed of diffusion of the ASF epidemic in Mainland China. The TSA method uses the polynomial expansion of the geographical coordinate of ASF cases to fit a multiple linear regression model through the least squares method (to ensure the minimum sum of the squared deviations from the trend surface) [19].

The general model for a given location was decomposed into a trend component and an error component and is given by the following:

$$T_i(X_i, Y_i) = \hat{T}_i(X_i, Y_i) + \varepsilon_i. \tag{3}$$

where  $(X_i, Y_i)$  is the geographic coordinates of individual case-points  $i$ ;  $T_i(X_i, Y_i)$  (in days) is the reported time of  $i$ , which was obtained based on the symptom onset date, with the first reported case of ASF as the baseline date;  $\hat{T}_i(X_i, Y_i)$  is the fitted time determined with TSA;  $\varepsilon_i$  is the associated error term at the  $i$ th location, indicating the deviation between the actual time of onset of the case and the time fitted by the trend surface analysis [20].

The relationship  $\hat{T}(X, Y)$  with  $X$  and  $Y$  is described using a generalized polynomial model:

$$\hat{T}(X, Y) = \sum_{l=0}^p \sum_{m=0}^p \beta_{lm} X^l Y^m. \tag{4}$$

where  $p$  is the order of the polynomial;  $\beta_{lm}$  are the polynomial coefficients, which are determined using least-squares regression to reduce the deviation in the surface trend surface and reported data to the greatest extent.

The core of a trend surface analysis is to calculate the trend surface from actual observations, and to use the regression analysis method to minimize the sum of squares of the residuals  $Q$ . The formula for deviation  $Q$  is as follows:

$$Q = \sum_{i=1}^n \varepsilon_i^2 = \sum_{i=1}^n [T_i(X_i, Y_i) - \hat{T}_i(X_i, Y_i)]^2. \tag{5}$$

The shape and flexibility of the trend surface depends on the order of the polynomial selected as a model [19]. The first-order polynomial limits the trend to a plane based on the data. The second-order polynomial model allows for some curvature on the entire data set, while the high-order model allows for more local curvature in the fitting surface. The order of the polynomial is determined by statistically evaluating the improvement in the model's fit as one moves from a lower order to a higher order [20]. The results of the trend surface analysis are used to generate outlines or smooth surfaces. Each contour line represents the specific prediction time period in the city's landscape settings since the initial invasion of ASF virus.

At the same time, we use the TSA fitted model to estimate the local direction and speed of diffusion of the epidemic at each set of location coordinates. Specifically, by calculating the partial derivative  $(\frac{\partial \hat{T}(X, Y)}{\partial X}, \frac{\partial \hat{T}(X, Y)}{\partial Y})$  of time  $\hat{T}(X, Y)$  with respect to coordinates  $X$  and  $Y$  and by substituting the geographic coordinate  $(X_i, Y_i)$  of the case  $i$ , we can obtain the local vector  $(\frac{\partial \hat{T}(X_i, Y_i)}{\partial X_i}, \frac{\partial \hat{T}(X_i, Y_i)}{\partial Y_i})$ , which represents the local transmission direction of case  $i$ ; the

local transmission speed is the reciprocal of the slope along the transmission direction, the square root of the speed is plotted on the map as vector arrows [21,22]. Specifically, all the analyses are performed in SPSS 22.0 software. Maps of the time contours and vectors were generated in ArcGIS 10.2.

**Kriging Interpolation.** To better explore the local spatial variation in ASF spread in Mainland China, we use kriging interpolation, a local spatial prediction method, to generate an estimated continuous surface and to predict the values of the time period using the surrounding, known scattered set of point values (i.e.,  $T$ ). Kriging is a local statistical interpolation method based on linear regression. This method determines the best combination of weights to interpolate the data points by minimizing the variance as derived from the spatial covariance in the data [23,24].

The formula for a general kriging interpolation is as follows:

$$T_0^*(X_0, Y_0) = \sum_{i=1}^n \omega_i T_i(X_i, Y_i). \tag{6}$$

where  $(X_i, Y_i)$  is the geographic coordinates of individual case-points  $i$ ;  $T_i(X_i, Y_i)$  (in days) is the reported time of  $i$ , which is obtained based on the symptom-onset date, with the first reported case of ASF as the baseline date;  $T_0^*(X_0, Y_0)$  is the predicted onset time for geographic location  $(X_0, Y_0)$ ; and  $\omega_i$  is the unknown weight, often referred to as the kriging weight. This weight is a set of optimal coefficients that can satisfy the minimum difference between the estimated and real onset dates at the geographical position  $(X_0, Y_0)$ , that is, when  $E[T_0(X_0, Y_0) - T_0^*(X_0, Y_0)] = 0$  is satisfied, the variogram function  $Var[T_0(X_0, Y_0) - T_0^*(X_0, Y_0)]$  is at the minimum.

Although kriging and a trend surface analysis have some common features in describing the overall spatial trend, the local interpolation performed by kriging can show the image enhancement of the local spatial model because the value of kriging is very close to the observed value.

**Global spatial isolation and exposure.** The isolation index is mainly used to measure the degree of contact between individuals with the same attribute in a space [25]. For example, this index can be used to depict the mean degree of contact (during pig transportation) between infected individuals (sites). The mathematical expression for the isolation index is as follows:

$$I.I = \frac{\frac{1}{\hat{I}} \sum_{i=1}^k \frac{I_i^2}{N_i}}{\frac{\hat{I}}{\hat{N}}} \tag{7}$$

in which  $i = 1, 2, \dots, k$ .  $k$  means the total number of regions studied;  $I_i$  serves as the sum of infected individuals  $I$  in the  $i$ th region;  $N_i$  is the total number of individuals in the  $i$ th region;  $\hat{I}$  is the total number of individuals  $I$  that were infected in the whole studied space;  $\hat{N}$  means the total number of individuals in the whole studied space; and  $\frac{1}{\hat{I}} \sum_{i=1}^k \frac{I_i^2}{N_i}$  is the probability of being infected after exposure to any infected individual  $I_i$ , taken at random.

The exposure index is mainly used to measure the degree of contact between individuals with different attributes within a space [26]. For example, the index is used to characterize the average degree of contact (during pig transportation) between susceptible individuals (sites) and infected individuals (sites). The mathematical expression for the exposure index is as follows:

$$E.I = \frac{\frac{1}{\hat{S}} \sum_{i=1}^k \frac{S_i I_i}{N_i}}{\frac{\hat{I}}{\hat{N}}} \tag{8}$$

where  $i = 1, 2, \dots, k$ ,  $k$  means the total number of regions studied;  $S_i$  serves as the sum of susceptible individuals  $S$  in the  $i$ th region;  $I_i$  is the total number of infected individuals  $I$  in the  $i$ th region;  $N_i$  represents the total number of individuals in the  $i$ th region;  $\hat{S}$  means the

total number of susceptible individuals  $S$  in the whole studied space;  $\hat{I}$  is the total number of infected individuals  $I$  in the whole studied space;  $\hat{N}$  is the total number of individuals in the whole studied space; and  $\frac{1}{\hat{S}} \sum_{i=1}^k \frac{S_i I_i}{N_i}$  is the probability of being infected after exposure to any susceptible individual  $S_i$ , taken at random.

**Local spatial isolation and exposure.** The local isolation and exposure represent the average degree of contact between individuals with the same attribute and different attributes in a local area, respectively [25–27]. According to the definition and formula of isolation and exposure indexes above, the mathematical expression of isolation index that reflects the infected individual in the  $i$ th area is as follows:

$$I.I(i) = \frac{\frac{1}{\hat{I}} \frac{I_i I_i}{N_i}}{\frac{\hat{I}}{\hat{N}}} \tag{9}$$

The mathematical expression of the exposure index of infected individuals in the  $i$ th region is as follows:

$$E.I(i) = \frac{\frac{1}{\hat{S}} \frac{S_i I_i}{N_i}}{\frac{\hat{I}}{\hat{N}}} \tag{10}$$

where the meaning of the variables is identical to the definitions above.

Specifically, all the numerical calculations are run in Matlab R2021 and the results are visualized in ArcGis 10.2.

### 3. Results

#### 3.1. Epidemiological Characteristics of ASF

First, the epidemiological characteristics in space and time were analyzed by sorting out and visualizing the collected African swine fever cases data.

Figure 2a shows the spatial distribution of African swine fever at the province level in Mainland China from 1 August 2018 to 31 August 2019. We find that African swine fever has spread across 31 provinces, autonomous regions, and municipalities directly under the central government in Mainland China, and the cases are mainly distributed in Liaoning Province, Guizhou Province, Yunnan Province, and Hainan Province, with the number of cases in other provinces being low. Figure 2b shows the spatial distribution of African swine fever at the city level in Liaoning Province during this period. The cases are mainly distributed in Dalian, Yingkou, Panjin, Anshan, Jinzhou, Shenyang, and Tieling in Liaoning Province. We find that these seven cities are clustered on the map, with a high number of cases in Shenyang and Yingkou and a low number in other cities.

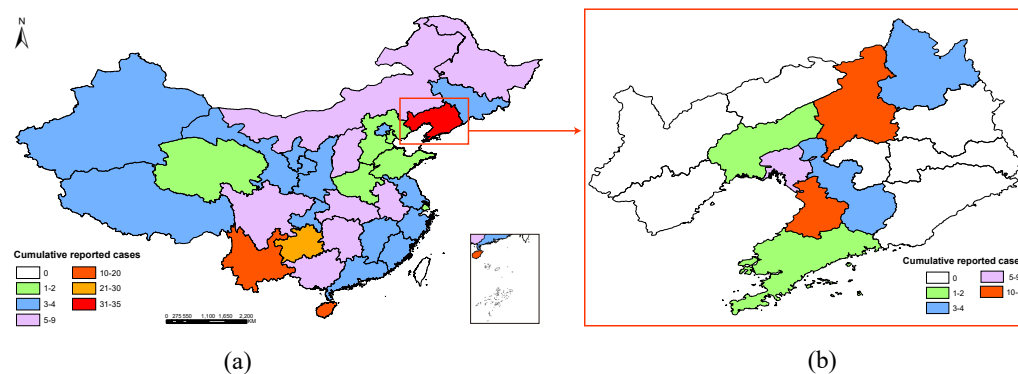


**Figure 2.** From 1 August 2018 to 31 August 2019: (a) Spatial distribution of incidence of ASF at the province level in Mainland China. (b) Spatial distribution of incidence of ASF at the city level in Liaoning Province.

Figure 3 shows a heat map of the surveillance data for ASF by province in Mainland China from 1 August 2018 to 31 August 2019. The results show that the number of ASF cases was high from August to December 2018, as well as the single-digit distribution; in April and June 2019, the number of cases increased again. On the whole, the ASF cases in all provinces occurred intermittently.

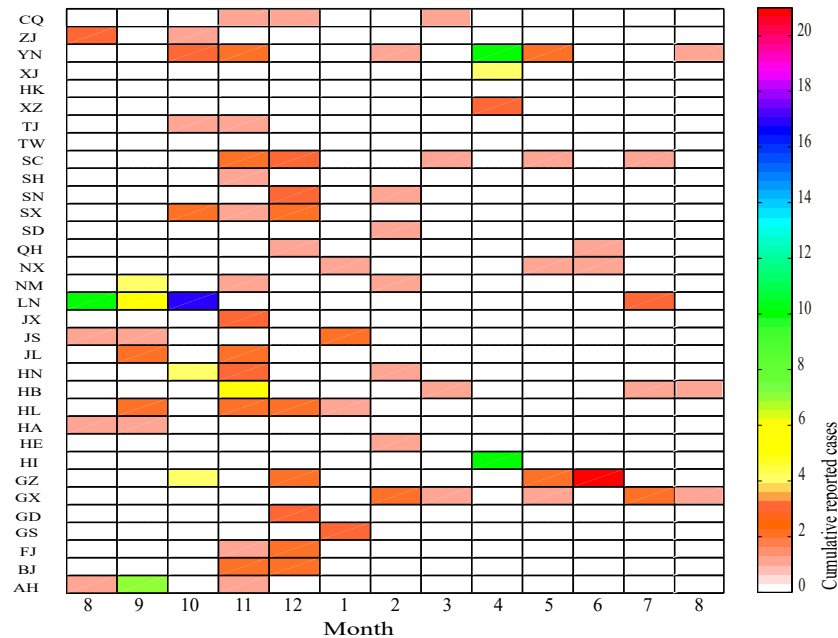


Figure 3. Heat map of surveillance data for ASF by province in Mainland China.

### 3.2. Spatial Distribution Characteristics of ASF

#### 3.2.1. Spatial Distribution Pattern

First, global Moran’s *I* statistics were obtained to determine the global spatial autocorrelation among ASF cases at the city level in Mainland China, shown in Table 1. The results show that the Z-score is greater than 1.96, and the *p*-values are significant at 0.05, which indicates that ASF cases are not randomly distributed and that global independence exists between ASF cases in Mainland China. Moreover, the global Moran *I* value is greater than zero, which indicates a positive correlation, and the distribution of ASF cases is influenced by space. Therefore, a spatial clustering analysis of ASF has been studied further.

Table 1. Result of the spatial autocorrelation test on ASFV cases in mainland of China, from 1 August 2018 to 31 August 2019.

Moran’s <i>I</i>	Expected <i>I</i>	Variance	Z-Score	<i>p</i> -Value	Result
0.028784	−0.002653	0.000114	2.940177	0.003280	clustered

#### 3.2.2. Cluster and Outlier

Local Moran’s *I* statistics are obtained to describe the distribution patterns of ASF cases at the city level in Mainland China and at the district or county level in Liaoning Province, which is shown in the Figure 4.

Figure 4a gives the cluster and outlier locations of ASF cases at the city level in Mainland China. Three distribution patterns are found for ASF cases: high–high cluster (HH), high–low outlier (HL), and low–high outlier (LH). The primary distribution mode is HH (blue), which are mostly located in Tieling, Shenyang, Panjin, Yingkou, and Anshan City in Liaoning Province; Bijie and Guiyang City in Guizhou Province; Nyingchi City in the Tibet Autonomous Region; and Haikou City in Hainan Province. The number of ASF cases in these cities and their surrounding cities is relatively high, and we should strengthen disease

prevention and control in and around these regions. The HL outliers (orange) are located in Huanggang City in Hubei Province, Diqing Tibetan Autonomous Prefecture in Yunnan Province, and Buyi and Miao Autonomous Prefecture of QianNan in Guizhou Province, indicating that the number of ASF cases in these three cities are higher than that of the surrounding cities. Therefore, in order to prevent the spread of the epidemic in these cities to the surrounding cities, we suggest that the government strictly prohibit the transportation of pigs and pig products from these cities to surrounding cities. The distribution of LH outliers (green) is only located in Liaoyang City, Liaoning Province, which means that the number of African swine fever cases in this city is lower than that in surrounding cities. We should do a good job in the detection and prevention of African swine fever in these cities and strictly prevent the importation of pigs and pig products. Zero number of African swine fever cases in other cities indicates no statistically significant data or random distribution.

Figure 4b shows the cluster and outlier locations of ASF cases at the district or county level in Liaoning Province. Two distribution patterns can be seen for African swine fever cases: high–high cluster (HH) and high–low outlier (HL). The HH concentration area (blue) is located in Dawa district of Panjin City, indicating that more cases of African swine fever are found in this area and surrounding areas. The HL outlier (orange) is located in Shenbei New District in Shenyang City, which indicates that the number of ASF cases in the the district is higher than that of the surrounding districts. For these districts showing HH cluster and HL characteristics, we recommend that similar prevention and control measures to those determined from the cluster and outlier analysis for ASF cases at the city level in Mainland China.

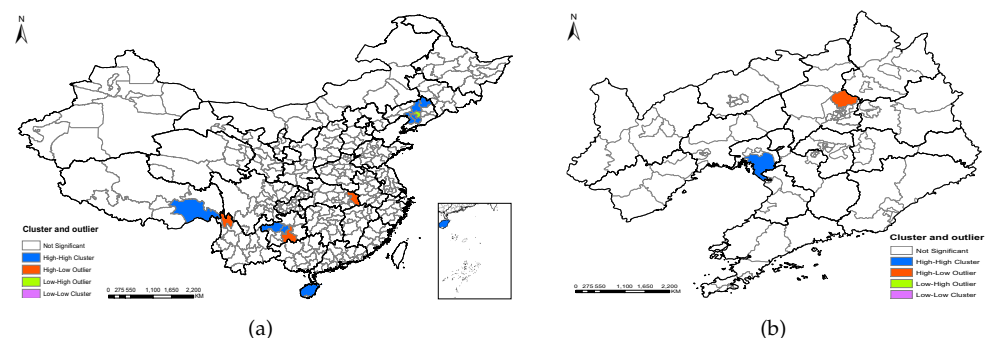


**Figure 4.** From 1 August 2018 to 31 August 2019: (a) Local indicators of spatial association (LISA) maps for the incidence of ASF at the city level in Mainland China. (b) Local indicators of spatial association (LISA) maps at the district or county level in Liaoning Province.

### 3.2.3. Hot Spots and Cold Spots

We used the Getis–Ord  $G_i^*$  index to analyze the hot spot distribution of ASF cases at the city level in Mainland China and at the district or county level in Liaoning Province, which is shown in Figure 5.

Figure 5a presents the hot and cold spots for ASF cases at the city level in Mainland China. Three hot spots ( $p < 0.05, |Z| > 1.96$ ) can be seen. One hot spot, mainly centered in Northeast China, included Liaoning Province; Tonghua, Liaoyuan, Siping, and Songyuan City in Jilin Province; Chifeng and Tongliao City in the Inner Mongolia Autonomous Region; and Qinhuangdao City in Hebei Province. The other two hot spots occurred in Southwest China, including Wenshan and Kunming City in Yunnan Province; Baise, Hechi, Chongzuo, Fangchenggang, Qinzhou, Nanning, Laibin, and Guigang City in the Guangxi Zhuang Autonomous Region; and Linzhi and Lvdu City in the Tibet Autonomous Region. These observations suggest that these areas have a relatively high number of ASF cases, resulting in a spatial high-value cluster distribution.

Figure 5b shows the hot and cold spots of ASF cases at the district or county level in Liaoning Province. The hot spots are mostly located Yingkou City, Dawa District in Panjin City, and Haicheng City in Anshan City. This observation means that the number of ASF

cases in these regions is relatively high, resulting in a spatial cluster distribution. We need to strengthen the prevention and control of ASF in these hot spots and surrounding areas.

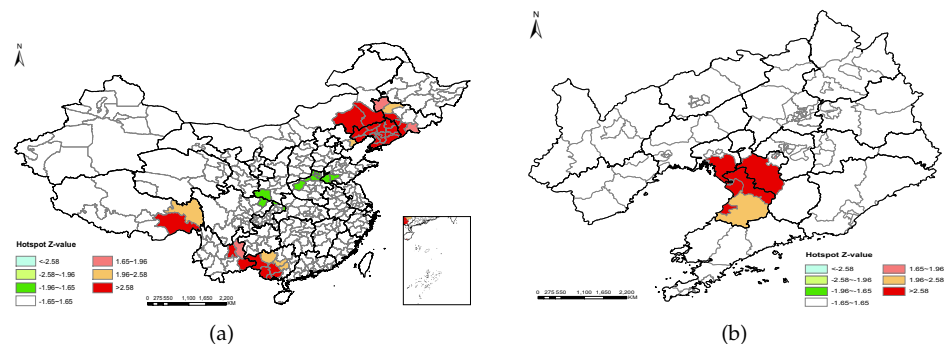


**Figure 5.** From 1 August 2018 to 31 August 2019: **(a)** Hot spot maps for the incidence of ASF at the city level in Mainland China. **(b)** Hot spot maps for the incidence of ASF at the district or county level in Liaoning Province.

### 3.3. Spatiotemporal Clustering Analysis

From the above spatial autocorrelation analysis, we determined that African swine fever cases showed spatial clustering characteristics in Mainland China from 1 August 2018 to 31 August 2019. Next, we used Kulldorff's space–time scan statistic method to detect the spatiotemporal clusters of ASF cases and to study the aggregation time and corresponding aggregation region of ASF cases at the municipal level in Mainland China and at the county or district level in Liaoning Province.

Table 2 lists the parameters of the significant spatiotemporal clusters of ASF cases at the city level in Mainland China, and Figure 6a gives a visual representation of these clusters. During the spatiotemporal scan analysis, the spatial unit was a city, with 374 cities in Mainland China, and the temporal unit was a day, with 395 days from 1 August 2018 to 31 August 2019. We selected a spatial window covering 20% of the total number of pig farms at risk and a temporal window covering 15% of the overall study period in order to scan small to large clusters. Monte Carlo was randomly set to 999. The results show that a most likely cluster area and six secondary cluster areas were detected in Mainland China during the study period. The most likely spatiotemporal cluster area only includes the Buyi and Miao Autonomous Prefecture of QianNan in Guizhou Province and the high-risk date was from 19 June 2019 to 25 June 2019 ( $RR = 2886.34, p < 0.001$ ). The first secondary spatiotemporal cluster areas were mainly centered in Anshan City (41.156280 N, 123.131015 E) in Liaoning Province, with a radius of 106.59 km covering five cities (Shenyang, Yingkou, Panjin, Anshanm and Liaoyang) in Liaoning Province, and the high-risk date was from 1 August 2018 to 10 October 2018 ( $RR = 182.05, p < 0.001$ ). The other four secondary spatiotemporal clusters are distributed in South China, Southwest China, North China, and several relatively small regions in Central China. Additionally, the cluster times varied with the cluster areas; more specific results are shown in Table 2 and Figure 6a. This indicates that the number of African swine fever cases in these areas is relatively high, forming a spatial clustering distribution for the corresponding times.

Table 3 lists the parameters of the significant spatiotemporal clusters of ASF cases at the district or county level in Liaoning Province, and Figure 6b gives a visual representation of these clusters. In the space–time scan analysis, the spatial unit is districts or counties, with 107 districts or counties in Liaoning Province; the temporal unit is again days, with 395 days from 1 August 2018 to 31 August 2019. We selected a spatial window covering 10% of the total number of pig farms at risk and a temporal window covering 10% of the overall study period in order to scan small to large clusters. Monte Carlo was randomly set to 999. The results show that a most likely cluster area and two secondary cluster areas are detected in Liaoning Province during the study period. The most likely spatiotemporal

cluster area is centered in Dawa District (40.958400 N, 122.105000 E) in Panjin City, with a radius of 52.63 km covering nine districts or counties, including all (four) districts or counties in Panjin City, four districts or counties (Xishi, Zhanqian, Laobing, and Dashiqiao Districts) in Yingkou City, and Taian County in Anshan City, and the high-risk date was from 26 September 2018 to 16 October 2018 ( $RR = 337.50, p < 0.001$ ). The secondary cluster 1 area is mainly located in Hunnan District (41.921700 N, 123.681000 E) in Shenyang City, with a radius of 24.27 km covering nine districts or counties (six in Shenyang City and three in Fushun City), and the high-risk date was from 8 August 2018 to 14 August 2018 ( $RR = 1242.38, p < 0.001$ ). Secondary cluster 2 is mainly centered in Changtu County (42.993600 N, 123.935000 E), with a radius of 72.03 km covering six districts or counties (five in Tieling City and Kangping County in Shenyang City), and the high-risk date was from 24 July 2019 to 30 July 2019 ( $RR = 547.73, p < 0.001$ ). These observations indicate a relatively high number of ASF cases in these regions, resulting in a spatial cluster distribution over the corresponding times.

**Table 2.** Results of the spatiotemporal cluster test on ASF cases at the city level in Mainland China from 1 August 2018 to 31 August 2019.

Cluster Type	Cluster Time Frame	Coordinates/Radius (km)	Cities (n)	RR	LLR	p-Value
Most likely cluster	19 June 2019–25 June 2019	(26.284520 N, 107.257580 E)/0	1	2886.34	138.32	<0.001
Secondary cluster1	1 August 2018–10 October 2018	(41.156280 N, 123.131015 E)/106.59	5	182.05	119.85	<0.001
Secondary cluster2	3 April 2019–10 April 2019	(29.110541 N, 95.458920 E)/406.86	4	24,267.31	117.83	<0.001
Secondary cluster3	29 August 2018–11 September 2018	(31.544085 N, 118.625382 E)/160.91	12	200.92	38.57	<0.001
Secondary cluster4	7 November 2018–27 November 2018	(30.319164 N, 114.792200 E)/59.46	4	3609.70	35.90	<0.001
Secondary cluster5	17 April 2019–23 April 2019	(22.126148 N, 113.574880 E)/502.52	38	223.62	35.16	<0.001
Secondary cluster6	21 November 2018–11 December 2018	(37.937164 N, 112.328130 E)/523.88	59	19.37	19.93	<0.001

**Table 3.** Results of the spatiotemporal cluster test on ASF cases at the district or county level in Liaoning Province from 1 August 2018 to 31 August 2019.

Cluster Type	Cluster Time Frame	Coordinates/Radius (km)	Districts(n)	RR	LLR	p-Value
Most likely cluster	26 September 2018–16 October 2018	(40.958400 N, 122.105000 E)/52.63	9	337.50	83.34	<0.001
Secondary cluster1	8 August 2018–14 August 2018	(41.921700 N, 123.681000 E)/24.27	9	1242.38	42.07	<0.001
Secondary cluster2	24 July 2019–30 July 2019	(42.993600 N, 123.935000 E)/72.03	6	547.73	15.79	<0.001

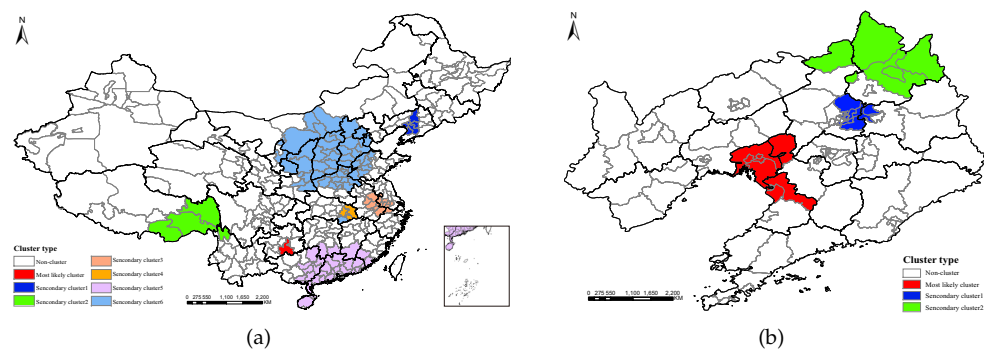


**Figure 6.** From 1 August 2018 to 31 August 2019: (a) Spatiotemporal clusters of ASF cases at the city level in Mainland China. (b) Spatiotemporal clusters of ASF at the district or county level in Liaoning Province.

### 3.4. The Direction and Speed of Diffusion of ASF

#### 3.4.1. Global Direction and Speed of Diffusion

We establish a bivariate polynomial regression function  $\hat{T}_i(X_i, Y_i)$  in the trend surface model  $T_i(X_i, Y_i)$ , in which the geographical location coordinates of the case are taken as independent variables and the onset time of the case is taken as a function of its geographical coordinates, which is a dependent variable. The order of the polynomial is determined by improving the fit of the statistical evaluation model from low to high order.  $\hat{T}_i(X_i, Y_i)$

uses a linear model (to determine the inclination plane) for the regression on geographic coordinates  $(X_i, Y_i)$ , adds quadratic terms (to identify any distortion in the direction) and then cubic terms (to show depressions or peaks on the diffused surface), and selects a cubic model of the trend surface based on the fit ( $R^2 = 0.385; p < 0.0001$ ) of the model. Quartic terms are entered into the model but do not add significance to the model fit. The final model took the following form:

$$T(X, Y) = 857.811 + 1.282X - 24.396Y - 4.646X^2 - 69.310XY - 6.914Y^2 - 0.923X^2 - 0.85X^2Y - 7.745Y^2X + 0.004Y^3. \tag{11}$$

The contoured trend-surface map (see Figure 7) shows the global direction and propagating wave of ASF in Mainland China from 1 August 2018 to 31 August 2019. Each contour line (black dashed line) represents a 30-day period. The edges of the contour lines means the direction of diffusion. If the contours are far apart, the disease spreads rapidly in an area. If the contours are close, the disease progresses slowly. The result shows that ASF spreads from northeastern to southwestern and then to western China. The disease spread was slower during the first 90 days (1 August to 31 October 2018) and was mainly distributed in Liaoning Province, Jilin Province, Heilongjiang Province, Shandong Province, Zhejiang Province, Jiangsu Province, and Anhui Province. The same pattern of disease spread occurred during days 180–240 (1 February to 31 March 2019) and was mainly distributed in Yunnan Province, Guizhou Province, Hunan Province, and the Guangxi Zhuang Autonomous Region; more specific results are shown in Figure 7.

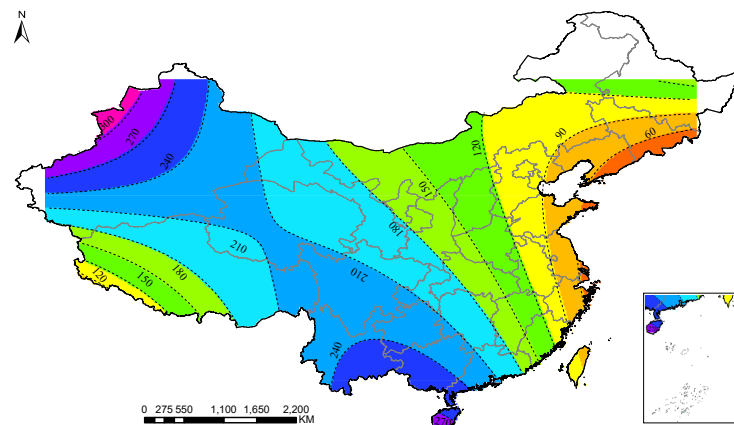


**Figure 7.** Contour map of the predicted spreading waves and velocity vector arrows of each case of ASF in Mainland China.

### 3.4.2. Local Direction and Speed of Diffusion

In order to visualize the instantaneous diffusion velocity at each set of position coordinates, the partial derivatives are calculated from the final model. The partial derivatives from the model are as follows:

$$\begin{aligned} \frac{\partial T(X, Y)}{\partial X} &= 1.282 - 9.292X - 69.310Y - 2.769X^2 - 1.6XY - 7.745Y^2, \\ \frac{\partial T(X, Y)}{\partial Y} &= -24.396 - 69.310X - 13.828Y - 0.85X^2 - 15.49YX + 0.012Y^2. \end{aligned} \tag{12}$$

By substituting the geographic coordinates of each case into Equation (12), we can determine the local propagation direction and speed of each case. ArcGIS 10.2 was used to visualize the local transmission direction and speed of each case. Detailed results are shown in Figure 7. The black arrow in the figure represents the instantaneous vector speed of the case at the geographical location.

### 3.4.3. Local Spatial Propagation Prediction

By means of kriging interpolation, we show the spatial forecast of ASF transmission in Mainland China from 1 August 2018 to 31 August 2019 in Figure 8. In the figure, different colors represents different periods (days); for example, the black dots represent ASF cases that have been monitored and the green pentagram represents the geographical location of the first case discovered. Furthermore, the isolines obtained from the trend surface analysis were applied to the figure to facilitate the comparison of the two results. As a result, the overall transmission trend is similar to that obtained from the trend surface analysis, namely, ASF spreading from the northeast to the southwest and then to the west. However, the results of location onset obtained by the kriging interpolation are not only more accurate than that by the trend-surface analysis but also more consistent with the veritable onset monitored locally. For the first 61 days (from 1 August 2018 to 30 September 2018), we see that the occurrence of ASF was more common in some areas of Liaoning Province, Zhejiang Province, Jiangsu Province, Anhui Province, and the Inner Mongolia Autonomous Region, while for the period from days 335 to 392 (from 1 July 2019 to 26 August 2019), a more intensive contagion is seen in some locations, such as the Guangxi Zhuang Autonomous Region, Sichuan Province, Hubei Province, and Liaoning Province. These locations at different time periods are also shown in the map, indicating a higher risk of infection during those periods, detailed in Figure 8.

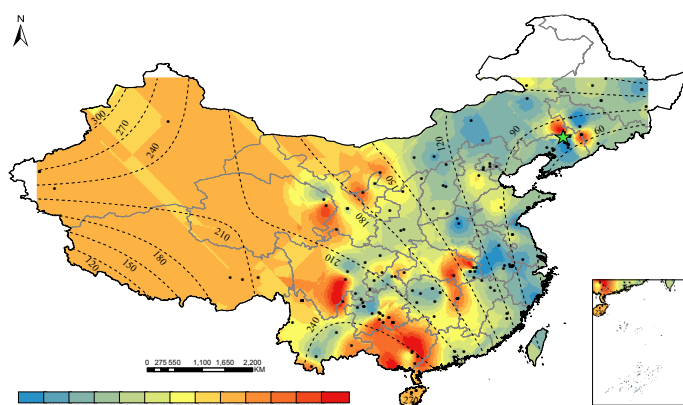


**Figure 8.** Spatial prediction map for the ordinary kriging interpolation of the duration of ASF spread in Mainland China.

### 3.5. Spatial Isolation and Exposure

#### 3.5.1. Global Spatial Isolation and Exposure

Based on the collected data of African-swine-fever-infected pig farms in each province and the total number of pig farms, we calculated and plotted the trend of isolation and exposure of African-swine-fever-infected sites in all of Mainland China from 1 August 2018 to 31 August 2019, shown in Figure 9. Figure 9a shows greater isolation values for the infected sites in November and December of 2018 and in April of 2019, which indicates a greater average degree of contact among infected sites in Mainland China at this time. This result coincides with the higher total number of cases reflected by the data obtained from monitoring during this period. Figure 9b shows lower exposure values of the infected sites in August of 2018, as well as in January, March, and August of 2019, which indicates less average exposure between susceptible sites and infected sites in Mainland China at this time. In other words, the risk of infection at healthy sites is lower during this time. This result coincides with the lower total number of cases reflected by the data obtained from monitoring during this period.

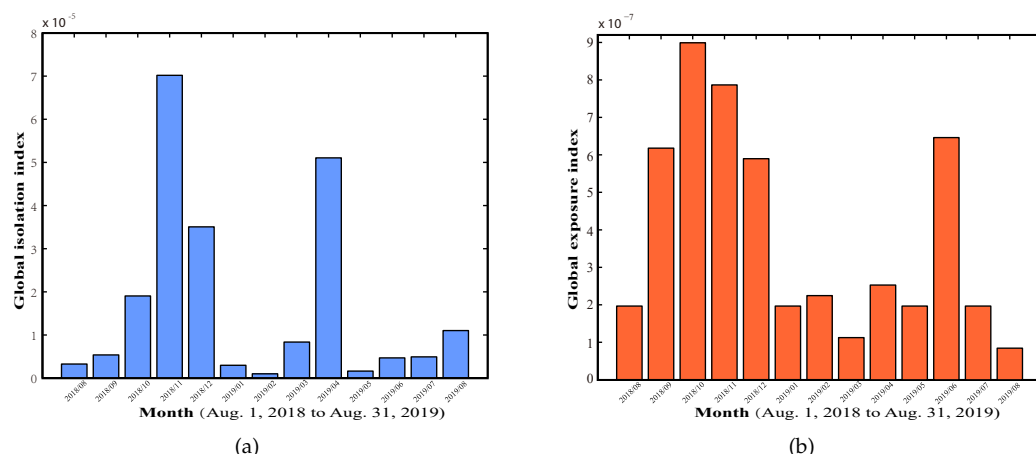


**Figure 9.** (a) Global isolation index of ASF cases from 1 August 2018 to 31 August 2019. (b) Global exposure index of ASF cases from 1 August 2018 to 31 August 2019.

### 3.5.2. Local Spatial Isolation and Exposure

Based on the collected data for infected sites of ASF in the provinces and the total number of pig farms, we calculated the local isolation and exposure of the infected sites in the provinces of Mainland China from 1 August 2018 to 31 August 2019, shown in Figure 10. Figure 10a shows greater isolation of the infected sites in Liaoning Province, Hubei Province, and Beijing, indicating greater average exposure in the infected sites in these regions. Figure 10b shows higher exposure of the infected sites in Liaoning Province and Hunan Province, which indicates higher average contact between the susceptible sites and the infected sites in these regions and a higher probability of infection in susceptible sites, but lower exposure of the infected sites in Shandong Province and Hebei Province, which indicates lower average contact between the susceptible sites and the infected sites in these regions and a lower probability of infection in healthy sites.

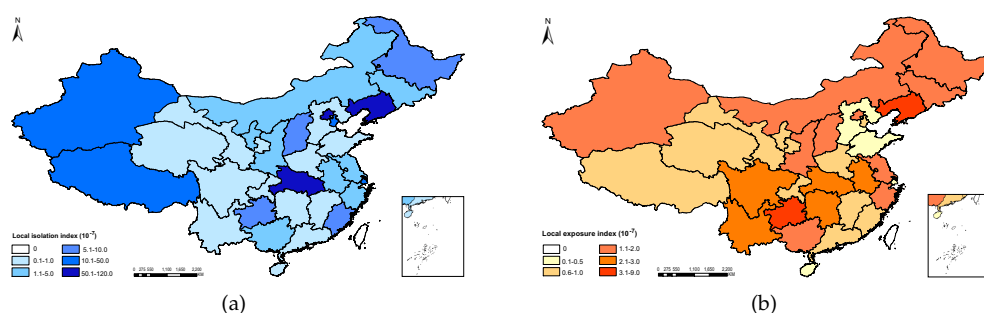


**Figure 10.** (a) Local isolation index of ASF cases from 1 August 2018 to 31 August 2019. (b) Local exposure index of ASF cases from 1 August 2018 to 31 August 2019.

## 4. Discussion

Since 2007, African swine fever has spread in many countries around the world, especially Russia and its surrounding areas. In March 2017, an African swine fever (ASF) outbreak occurred in Irkutsk Prefecture in the Russian Far East, which was only about 1000 km away from China [28]. On 3 August 2018, African swine fever was first confirmed in a pig farm in Shenbei New District, Shenyang City, Liaoning Province, China. According to identification by experts, the ASF virus that caused the outbreak in China belongs to the genotype II group and has about 99.95% homology with the whole genome sequence of the virus from Georgia, Russia and Poland [29]. Our study identified three ASF hot spots in Mainland China, which is indicative of a relatively high number of ASF cases in these areas. One is in the northeast region, including some cities in Liaoning Province,

Jilin Province, and the Inner Mongolia Autonomous Region. These areas are all located in frontier provinces in Northeast China, and the disease occurred at the early stages. These results indicate that we must strengthen the monitoring and management of entry–exit ports. The other hot spots include some parts of Southwest China, indicating the need to strengthen domestic trade and the transport of pigs and their products.

Spatiotemporal cluster analysis identified seven space–time cluster areas, including one most likely cluster area and six secondary clusters. The most likely spatiotemporal cluster area was Buyi and Miao Autonomous Prefecture of QianNan in Guizhou Province from 19 June 2019 to 25 June 2019. The first secondary spatiotemporal cluster area included Shenyang, Yingkou, Panjin, Anshan, and Liaoyang city in Liaoning Province, and the cluster time period was from 1 August 2018 to 10 October, 2018. The other four secondary spatiotemporal clusters were distributed in South China, Southwestern China, North China, and several relatively small areas in Central China. Analyzing Liaoning Province specifically, the author gives three space–time cluster areas that are more easily infected during the corresponding clustering time period. This result indicates a relatively high number of ASF cases in these areas, forming a spatial cluster distribution during the corresponding time period, and the prevention and control measures need to be strengthened.

For the direction of diffusion of African swine fever in China, Ma et al. revealed a trend of ASF spread in China in the northeast–southwest direction from August 1, 2018 to January 1, 2019 using the standard deviational ellipse (SDE) method [10]. In our study, using a trend surface analysis, we obtained the global and local transmission direction and speed of ASF in Mainland China and found that the spread route of ASF in Mainland China is from northeast to southwest and then west from 1 August 2018 to 31 August 2019. In addition, ASF slowly transmits from one place to another in the first three months and shows instantaneous transmission in terms of direction and speed at the infected sites.

Furthermore, the kriging spatial interpolation method gave a prediction of the period in which parts of Mainland China are at risk of ASF infection. Finally, using the isolation and exposure indexes, we calculated the global and local isolation and exposure of sites infected with ASF in Mainland China, revealing the infection risk at susceptible sites for different time periods and location. These study findings confirm that an analysis of the temporal and spatial transmission characteristics of African swine fever in China was needed.

However, some limitations were also present in this study. The analysis of the spatiotemporal transmission characteristics of African swine fever only provides a surface-level understanding of the data, and only a spatiotemporal statistical analysis was conducted based on the data, while the internal transmission mechanism of infectious diseases was not considered. How to integrate the transmission mechanism of infectious diseases into a spatiotemporal statistical analysis will be important work for future research.

## 5. Conclusions

In summary, this study revealed that the hot spots of ASF cases were mainly located in some cities in Northeast China, including Liaoning Province, Jilin Province, and the Inner Mongolia Autonomous Region. The most likely spatiotemporal cluster was concentrated in Buyi and Miao Autonomous Prefecture of QianNan in Guizhou Province, and the cluster date was from 19–25 June 2019. The first secondary cluster areas included five cities in Liaoning Province from 1 August to 10 October 2018. In addition, the time of infection at highest risk in local areas was predicted based on a kriging spatial interpolation, and the infection risk of susceptible pig farms and slaughterhouses at different time periods and location was revealed based on an isolation and exposure analysis. Our conclusions can provide a better understanding of this epidemic's trends. At the hot spots, spatiotemporal clusters, and space–time areas with high infection risks for African swine fever determined in this study, strengthening the prevention and control of disease transmission is necessary, for example, to strictly supervise the deep burial of dead and culled pigs and their related products; to disinfect contaminated and potentially contaminated articles, vehicles, and sites; and to strengthen the establishment and control of entry and exit checkpoints.

**Author Contributions:** Conceptualization, Z.J.; methodology, X.P.; software, X.P. and J.H.; writing—original draft preparation, X.P. and M.L.; writing—review and editing, J.H., J.Z. and Z.J.; project administration, X.P.; funding acquisition, X.P. and M.L. All authors have read and agreed to the published version of the manuscript.

**Funding:** This work is supported by the National Natural Science Foundation of China (grants 12101443, 61873154, 11971278 and 11801398), the Natural Science Foundation of Shanxi Province (grants 20210302124260, 202103021224095), the Preferential Funding for Science and Technology Activities for Returned Overseas Chinese Scholars of Shanxi province (grant 20210009), the Shanxi Scholarship Council of China (HGKY2019004), and the Scientific and Technological Innovation Programs (STIP) of Higher Education Institutions in Shanxi (2019L0082).

**Institutional Review Board Statement:** Not applicable.

**Informed Consent Statement:** Not applicable.

**Data Availability Statement:** Data are available in a publicly accessible repository.

**Acknowledgments:** The authors would like to thank the referees and editors for their very helpful and constructive comments, which have significantly improved the quality of this paper.

**Conflicts of Interest:** The authors declare no conflict of interest.

## Appendix A

### Appendix A.1. The Formula for global Moran’s $I$

The formula for global Moran’s  $I$  is as follows:

$$I = \frac{n \sum_{i=1}^n \sum_{j=1}^n \omega_{ij} (x_i - \bar{x})(x_j - \bar{x})}{(\sum_{i=1}^n \sum_{j=1}^n \omega_{ij}) \sum_{i=1}^n (x_i - \bar{x})^2}, i \neq j.$$

where  $i = 1, 2, 3, \dots, n$  and  $j = 1, 2, 3, \dots, n$ , where  $n$  is the number of cities, and districts or counties;  $x_i$  and  $x_j$  are the infectious cases in cities, and districts or counties  $i$  and  $j$ ;  $\bar{x}$  is the average number of infectious cases in the entire study area; and  $\omega_{ij}$  is a binary weighting matrix for the adjacent cities, and districts or counties  $i$  and  $j$  when the regions  $i$  and  $j$  are adjacent, with  $\omega_{ij} = 1$  and  $\omega_{ij} = 0$  otherwise.

The statistical significance of Moran’s  $I$  is evaluated using Monte Carlo tests with Z-score statistics, and the  $P$ -values are based on a permutation test. Z-score is calculated as follows:

$$Z = \frac{I - E[I]}{\sqrt{Var[I]}}$$

where  $E[I] = -\frac{1}{n-1}$  is the expected value of  $I$  and  $Var[I] = \sqrt{E[I^2] - E[I]^2}$  is the standard deviation.  $|Z| \geq 1.96, P < 0.05$  indicates statistical significance at the 5% level.

### Appendix A.2. The Formula for local Moran’s $I$

The formula for local Moran’s  $I$  is as follows:

$$I_i = \frac{x_i - \bar{x}}{\frac{1}{n-1} \sum_{j=1, j \neq i}^n (x_j - \bar{x})^2 - \bar{x}^2} \sum_{j=1, j \neq i}^n \omega_{ij} (x_j - \bar{x}).$$

The formula for  $Z_{I_i}$ -score is as follows:

$$Z_{I_i} = \frac{I_i - E[I_i]}{\sqrt{E[I_i^2] - E[I_i]^2}}$$

where  $E[I_i] = -\frac{1}{n-1}$  is the expected value of  $I_i$ .

### Appendix A.3. The Formula for Getis–Ord $G_i^*$

The formula for Getis–Ord  $G_i^*$  is as follows:

$$G_i^* = \frac{\sum_{j=1}^n \omega_{ij} x_j - \bar{x} \sum_{j=1}^n \omega_{ij}}{\sqrt{\frac{1}{n} \sum_{j=1}^n x_j^2 - \left(\frac{1}{n} \sum_{j=1}^n x_j\right)^2} \sqrt{\frac{n \sum_{j=1}^n \omega_{ij}^2 - \left(\sum_{j=1}^n \omega_{ij}\right)^2}{n-1}}}$$

## References

1. Normile, D. Arrival of deadly pig disease could spell disaster for China. *Science* **2018**, *361*, 741. [[CrossRef](#)] [[PubMed](#)]
2. Li, X.; Tian, K. African swine fever in China. *Vet. Rec.* **2018**, *183*, 300. [[CrossRef](#)] [[PubMed](#)]
3. Cliff, A.D.; Ord, J.K. *Spatial Processes: Models & Applications*; Taylor & Francis: Abingdon, UK, 1981.
4. Getis, A.; Ord, J.K. *The Analysis of Spatial Association by Use of Distance Statistics. Perspectives on Spatial Data Analysis*; Springer: Berlin/Heidelberg, Germany, 2010; pp. 127–145.
5. Anselin, L. Local indicators of spatial association—LISA. *Geogr. Anal.* **1995**, *27*, 93–115. [[CrossRef](#)]
6. Zakharova, O.I.; Titov, I.A.; Gogin, A.E.; Sevskikh, T.A.; Korennoy, F.I.; Kolbasov, D.V.; Abrahamyan, L.; Blokhin, A.A. African swine fever in the Russian Far East (2019–2020): Spatio-temporal analysis and implications for wild ungulates. *Front. Vet. Sci.* **2021**, *8*, 723081. [[CrossRef](#)] [[PubMed](#)]
7. Andrey, B.; Nadezhda, T.; Olga, B.; Timofey, S.; Andrey, G.; Olga, Z.; Zoran, D. Spatio-Temporal Analysis of the Spread of ASF in the Russian Federation in 2017–2019. *Acta Vet.-Beog* **2020**, *70*, 194–206. [[CrossRef](#)]
8. Shao, Q.; Li, R.; Han, Y.; Han, D.; Qiu, J. Temporal and Spatial Evolution of the African Swine Fever Epidemic in Vietnam. *Int. J. Environ. Res. Public Health* **2022**, *19*, 8001. [[CrossRef](#)] [[PubMed](#)]
9. Andraud, M.; Bougeard, S.; Chesnoiu, T.; Rose, N. Spatiotemporal clustering and Random Forest models to identify risk factors of African swine fever outbreak in Romania in 2018–2019. *Sci. Rep.* **2021**, *11*, 2098. [[CrossRef](#)]
10. Ma, J.; Chen, H.; Gao, X.; Xiao, J.; Wang, H. African swine fever emerging in China: Distribution characteristics and high-risk areas. *Prev. Vet. Med.* **2020**, *175*, 104861. [[CrossRef](#)]
11. Zhang, P.; Nie, T.; Ma, J.; Chen, H. Identification of Suitable Areas for African Swine Fever Occurrence in China Using Geographic Information System-based Multi-criteria Analysis. *Prev. Vet. Med.* **2022**, *209*, 105794. [[CrossRef](#)]
12. Dolan, C.; O’Halloran, A.; Bradley, D.G.; Croke, D.T.; Evans, A.; O’Brien, J.K.; Dicker, P.; Shields, D.C. Genetic stratification of pathogen-response-related and other variants within a homogeneous Caucasian Irish population. *Eur. J. Hum. Genet.* **2005**, *13*, 798–806. [[CrossRef](#)]
13. Sadeq, M. Spatial patterns and secular trends in human leishmaniasis incidence in Morocco between 2003 and 2013. *Infect. Dis. Poverty* **2016**, *5*, 1–13. [[CrossRef](#)] [[PubMed](#)]
14. Waldhör, T. The spatial autocorrelation coefficient Moran’s I under heteroscedasticity. *Stat. Med.* **1996**, *15*, 887–892. [[CrossRef](#)]
15. Wu, X.; Hu, S.; Kwaku, A.B.; Li, Q.; Luo, K.; Zhou, Y.; Tan, H. Spatio-temporal clustering analysis and its determinants of hand, foot and mouth disease in Hunan, China, 2009–2015. *BMC Infect. Dis.* **2017**, *17*, 645. [[CrossRef](#)] [[PubMed](#)]
16. Wong, W.S.D.; Lee, J. *Statistical Analysis of Geographic Information with ArcView GIS and ArcGIS*; Wiley: Hoboken, NJ, USA, 2005.
17. Kulldorff, M.; Huang, L.; Pickle, L.; Duczmal, L. An elliptic spatial scan statistic. *Stat. Med.* **2006**, *25*, 3929–3943. [[CrossRef](#)]
18. Kulldorff, M.; Feuer, E.J.; Miller, B.A.; Freedma, L.S. Breast cancer clusters in the northeast United States: A geographic analysis. *Am. J. Epidemiol.* **1997**, *146*, 161–170. [[CrossRef](#)]
19. Lucey, B.T.; Russell, C.A.; Smith, D.; Wilson, M.L.; Long, A.; Waller, L.A.; Childs, J.E.; Real, L.A. Spatiotemporal analysis of epizootic raccoon rabies propagation in Connecticut, 1991–1995. *Vector Borne Zoonotic Dis.* **2002**, *2*, 77–86. [[CrossRef](#)] [[PubMed](#)]
20. Moore, D.A.; Carpenter, T.E. Spatial analytical methods and geographic information systems: use in health research and epidemiology. *Epidemiol. Rev.* **1999**, *21*, 143–161. [[CrossRef](#)]
21. Moore, D.A. Spatial diffusion of raccoon rabies in Pennsylvania, USA. *Prev. Vet. Med.* **1999**, *40*, 19–32. [[CrossRef](#)]
22. Lizarazo, E.; Vincenti-Gonzalez, M.; Grillet, M.E.; Bethencourt, S.; Diaz, O.; Ojeda, N.; Ochoa, H.; Rangel, M.A.; Tamacorresponding, A. Spatial dynamics of Chikungunya virus, Venezuela, 2014. *Emerg. Infect. Dis.* **2019**, *25*, 672. [[CrossRef](#)]
23. Oliver, M.A.; Webster, R. Kriging: a method of interpolation for geographical information systems. *Int. J. Geogr. Inf. Sci.* **1990**, *4*, 313–332. [[CrossRef](#)]
24. Dale, M.R.T.; Fortin, M.J. *Spatial Analysis: A Guide for Ecologists*; Cambridge University Press: Cambridge, UK, 2014.
25. Bell, W. A probability model for the measurement of ecological segregation. *Soc. Forces* **1954**, *32*, 357–364. [[CrossRef](#)]
26. Gottman, J.M.; Coan, J.; Carrere, S.; Swanson, C. Predicting marital happiness and stability from newlywed interactions. *Soc. Forces* **1998**, *5*–22. [[CrossRef](#)]

27. Feitosa, F.F.; Camara, G.; Monteiro, A.M.V.; Koschitzki, T.; Silva, M.P.S. Global and local spatial indices of urban segregation. *Int. J. Geogr. Inf. Sci.* **2007**, *21*, 299–323. [[CrossRef](#)]
28. Kolbasov, D.; Titov, I.; Tsybanov, S.; Gogin, A.; Malogolovkin, A. African swine fever virus, Siberia, Russia, 2017. *Emerg. Infect. Dis.* **2018**, *24*, 796–798. [[CrossRef](#)] [[PubMed](#)]
29. Zhou, X.; Li, N.; Luo, Y.; Liu, Y.; Miao, F.; Chen, T.; Zhang, S.; Cao, P.; Li, X.; Tian, K.; et al. Emergence of African swine fever in China, 2018. *Transbound. Emerg. Dis.* **2018**, *65*, 1482–1484. [[CrossRef](#)] [[PubMed](#)]